

## Investigating Space Weathering Effects Using Coordinated Analysis of a H<sup>+</sup>- and He<sup>+</sup>-Irradiated Carbonaceous Chondrite

Dara Laczniak<sup>1</sup>, Michelle Thompson<sup>1</sup>, Catherine Dukes<sup>2</sup>, Richard Morris<sup>3</sup>, Simon Clemett<sup>3</sup>, Lindsay Keller<sup>3</sup> and Roy Christoffersen<sup>3</sup>

<sup>1</sup>Purdue University, West Lafayette, Indiana, United States, <sup>2</sup>University of Virginia, Charlottesville, Virginia, United States, <sup>3</sup>NASA Johnson Space Center, Houston, Texas, United States

Space weathering processes such as micrometeorite bombardment and solar wind irradiation alter the microstructural, compositional, and optical properties of airless body regoliths. As a result, space weathering complicates the interpretation of remote sensing data from spacecraft missions [1]. Unlike the Moon and asteroids similar in composition to unaltered ordinary chondrites, very little is known about space weathering of hydrated, organic-rich (carbonaceous or C-type) planetary bodies. In the next three years, the Hayabusa2 and OSIRIS-REx missions will return samples from C-type asteroids Ryugu and Bennu, respectively [2,3]. To maximize the scientific return of these missions, we simulated solar wind irradiation in the laboratory on CM2 Murchison—a suitable analog for C-type asteroids [4]. We present results from a coordinated analysis investigating how 1 keV/amu H<sup>+</sup> and He<sup>+</sup> ion irradiation modifies the physical, chemical, and spectral properties of the organic and inorganic components of carbonaceous chondrites.

H<sup>+</sup> and He<sup>+</sup> irradiations were performed separately under ultra-high vacuum on two discrete 6x6 mm regions of a dry-cut Murchison slice. Using a flux of  $1.1 \times 10^{13}$  ions/cm<sup>2</sup>/s, the first region was irradiated with 4 keV He<sup>+</sup> to a total fluence of  $1.1 \times 10^{18}$  ions/cm<sup>2</sup> (~6000 years of exposure at Bennu) while the second region was irradiated with 1 keV H<sup>+</sup> to a total fluence of  $8.1 \times 10^{17}$  ions/cm<sup>2</sup> (~200 years of exposure at Bennu). To comprehensively analyze the samples, we employed four analytical techniques: (1) X-ray photoelectron spectroscopy (XPS), (2) visible to near infrared (VNIR; 0.35–2.50 μm) spectroscopy, (3) two-step laser-desorption mass spectrometry (μL<sup>2</sup>MS), and transmission electron microscopy (TEM). We observed changes in surface chemistry via in situ XPS using a PHI Versaprobe with a monochromatic, scanning X-ray source (AlKα: 1486.7 eV) and hemispherical electron-energy analyzer. We collected VNIR spectra using a fiber-optic ASD FieldSpec 3 Spectrometer (Malvern Panalytical) under ambient laboratory conditions to understand trends in reflectance. Changes in organic functional group chemistry were evaluated using a 118 nm photoionization spectral map acquired with a μL<sup>2</sup>MS instrument. Using an FEI Quanta 3D focused ion beam scanning electron microscope (FIB-SEM), we prepared eight electron transparent thin sections consisting of matrix material, pyroxene, Mg-rich olivine, and Fe-rich olivine from both the H<sup>+</sup>- and He<sup>+</sup>-irradiated regions. TEM analysis of these FIB-sections revealed microstructural and chemical changes driven by ion irradiation. Specifically, we acquired bright field (BF), high-angle annular dark field (HAADF), and high-resolution TEM (HRTEM) images, as well as elemental distribution maps, using a JEOL 2500SE 200 kV field-emission scanning TEM equipped with a SDD 60 mm<sup>2</sup> thin window energy-dispersive X-ray spectrometer (EDX).

VNIR spectra indicate that He<sup>+</sup>-irradiation causes significant spectral brightening (increase in albedo) and reddening (increasing reflectance with increasing wavelength) while H<sup>+</sup>-irradiation does not. Both irradiated spectra show weakened ~1.0 (Fe<sup>2+</sup> silicates), ~0.7 (Fe<sup>2+</sup>-Fe<sup>3+</sup> phyllosilicates), and ~1.94 μm

(water) absorption bands [5].  $\text{He}^+$ -irradiation also slightly strengthens absorptions at  $\sim 0.47$  and  $\sim 0.50$   $\mu\text{m}$  bands (Fe-oxides). Both XPS spectra and  $\mu\text{L}^2\text{MS}$  organic maps show a decrease in overall organic concentration due to the destruction and preferential removal of free organic species (or the re-distribution of their atomic components by ion mixing or diffusion). XPS spectra also indicate that ion irradiation alters surface sulfate minerals to sulfides and chemically reduces surface  $\text{Fe}^{3+}$  to native  $\text{Fe}^{2+}$  and a small amount of  $\text{Fe}^0$ .

TEM analysis of the  $\text{He}^+$ -irradiated matrix FIB-section shows a continuous ion-affected vesiculated layer ( $>100$  nm) in which amorphization reaches 125–175 nm below the surface (Fig 1A). In the  $\text{H}^+$ -irradiated matrix FIB-section, the vesiculated layer is uniformly  $< 100$  nm thick and the amorphization depth does not exceed  $\sim 60$  nm (Fig 1B). The  $\text{He}^+$ -irradiated Mg-rich olivine FIB-section has an ion-affected region averaging  $\sim 85$  nm in thickness that is dominated by amorphous olivine with some polycrystalline areas (Fig 1C). In the  $\text{H}^+$ -irradiated Mg-rich olivine, the ion-affected layer is  $\sim 60$  nm thick and dominated by polycrystalline olivine with few amorphous islands (Fig 1D). Nanoparticles are only present in the vesiculated-amorphous layer of the  $\text{H}^+$ -irradiated pyroxene FIB-section (Fig 2). These nanoparticles have d-spacings consistent with an Fe-bearing phase (e.g., 0.15, 0.21, 0.22, and 0.24 nm), but the exact phase has not yet been determined. The  $\text{He}^+$ -irradiated Mg-rich olivine and  $\text{H}^+$ -irradiated pyroxene both possess a thin, dark, highly-strained boundary layer between the vesiculated-amorphous and crystalline regions, similar to that observed in Hayabusa particles [6,7].

Ion irradiation of carbonaceous material yields complex results. XPS and  $\mu\text{L}^2\text{MS}$  data show a net decrease of carbon associated with the alteration and removal of organics. XPS also shows a chemical reduction of iron and sulfides, which may indicate the production of Fe-bearing nanoparticles (Fe-oxides, Fe-sulfides,  $\text{Fe}^0$ ). Trends in reflectance also suggest nanoparticle formation. Irradiation-induced attenuation of the 0.7 and 1.0  $\mu\text{m}$  bands may reflect the breakdown of matrix phyllosilicates and/or the partial reduction of native iron [8]. The combination of absorption strengthening at 0.47 and 0.50  $\mu\text{m}$  ( $\text{Fe}^{3+}$  oxides) and absorption weakening at 1.94  $\mu\text{m}$  (OH/ $\text{H}_2\text{O}$ ) may reflect the formation of Fe-oxide nanoparticles via dehydrogenation in reducing environments [9]. Although XPS and reflectance results can be explained by minor nanoparticle formation, nanoparticles are not universally identified in the TEM analysis. Additional TEM analysis is underway to further investigate this paucity of nanoparticles and constrain interpretations from coordinated results [10].

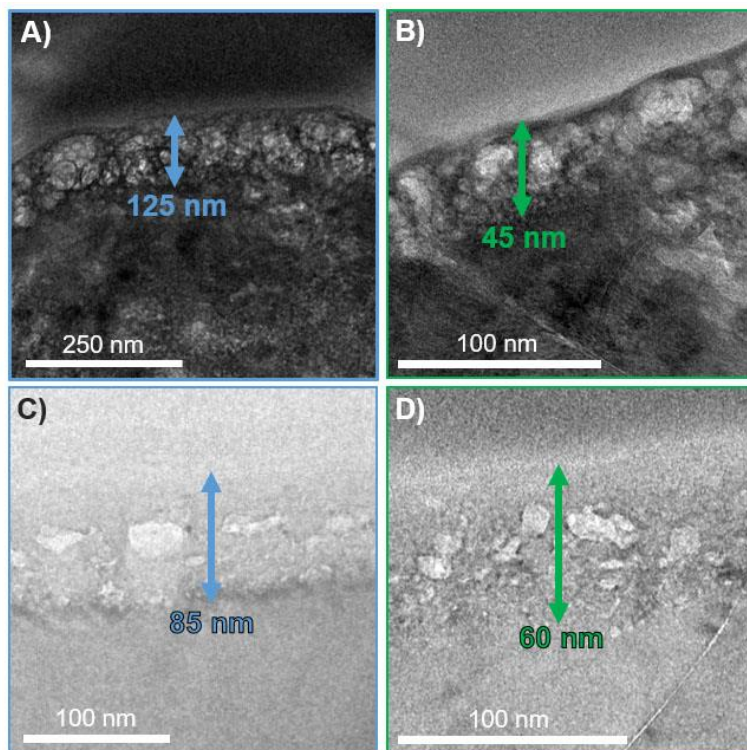


**Figure 1.** Conventional TEM images of (A) He<sup>+</sup>-irradiated matrix, (B) H<sup>+</sup>-irradiated matrix, (C) He<sup>+</sup>-irradiated Mg-rich olivine, and (D) H<sup>+</sup>-irradiated Mg-rich olivine. Arrows indicate thicknesses of ion-affected regions.

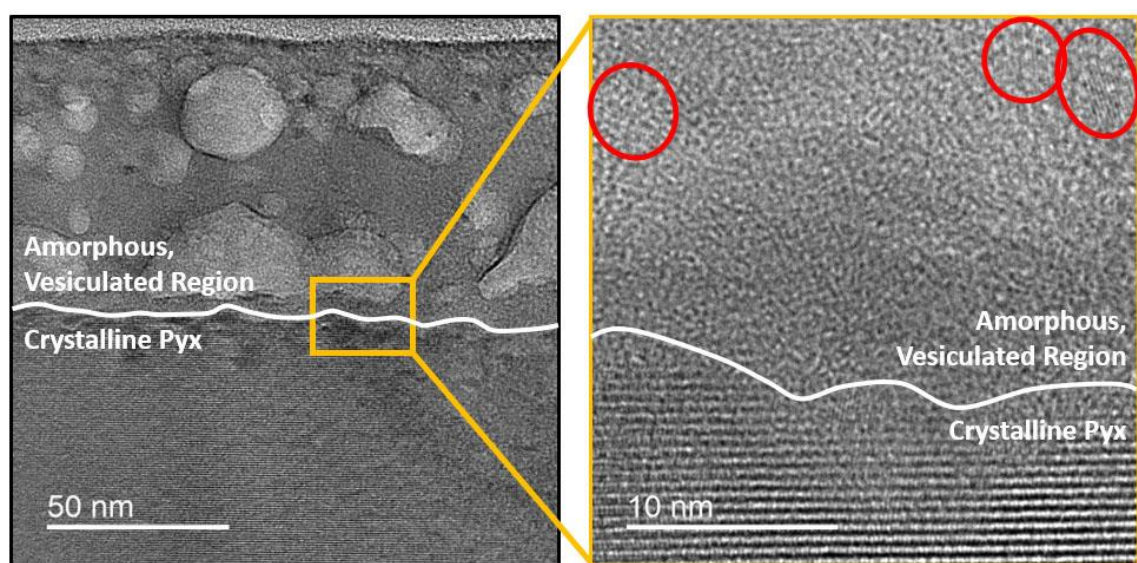


**Figure 2.** High-resolution TEM images showing the boundary between the amorphous, vesiculated layer and crystalline substrate in the H<sup>+</sup>-irradiated pyroxene FIB-section (left and right panels). Crystalline material is indicated by lattice fringes (i.e., atomic planes). Fe-bearing nanoparticles (outlined in red) are shown in the higher magnification call-out on the right.

#### References

- [1] C M Pieters and S K Noble, *Journal of Geophysical Research-Planets* **121** (2016), p. 1865.

- [2] D S Lauretta et al., *Nature* **568** (2019), p. 55.
- [3] K Kitazato et al., *Science* **364** (2019), p. 272.
- [4] B Clark et al., *Icarus* **216** (2011), p. 462.
- [5] E A Cloutis et al., *Icarus* **220** (2012), p. 586.
- [6] L P Keller and E L Berger, *Earth, Planets, & Space* **66** (2014), p. 71.
- [7] M S Thompson et al., *Earth, Planets, & Space* **66** (2014), p. 89.
- [8] L P Keller et al., 46<sup>th</sup> Lunar & Planetary Science Conference Proceedings (2015), p. 1913.
- [9] M S Thompson et al., 49<sup>th</sup> Lunar & Planetary Science Conference Proceedings (2018), p. 2408.
- [10] This research was supported by NASA grant 80NSSC19K0960.